Microfluid Nanofluid (2016) 20:46
DOI 10.1007/s10404-016-1713-6

RESEARCH PAPER

"Law of the nano-wall" in nano-channel gas flows

Murat Barisik[1] · **Ali Beskok**[2]

Received: 6 October 2015 / Accepted: 1 February 2016 / Published online: 23 February 2016

Abstract Molecular dynamics simulations of force-driven nano-channel gas flows show two distinct flow regions. While the bulk flow region can be determined using kinetic theory, transport in the near-wall region is dominated by gas–wall interactions. This duality enables definition of an inner-layer scaling, y^*, based on the molecular dimensions. For gas–wall interactions determined by Lennard–Jones potential, the velocity distribution for $y^* \leq 3$ exhibits a universal behavior as a function of the local Knudsen number and gas–wall interaction parameters, which can be interpreted as the "law of the nano-wall." Knowing the velocity and density distributions within this region and using the bulk flow velocity profiles from Beskok–Karniadakis model (Beskok and Karniadakis in Microscale Thermophys Eng 3(1):43–77, 1999), we outline a procedure that can correct kinetic-theory-based mass flow rate predictions in the literature for various nano-channel gas flows.

Keywords Wall force field effects · Scale effects · Nano-flows · Mass flow rate · Smart wall molecular dynamics

1 Introduction

Gas flows in nanoscale domains are observed in a wide range of applications including the magnetic disk drives (Tagawa et al. 2007; Juang et al. 2007), hydrogen storage units (Chalk and Miller 2006; Furukawa and Yaghi 2009; Cho et al. 2011), gas separation membranes (Li et al. 2011; Venna and Carreon 2009; Yave et al. 2010) and shale gas reservoirs (Loucks et al. 2009; Chong et al. 2010; Michel et al. 2011). These flows exhibit substantially different physics from continuum descriptions due to (1) *rarefaction*, (2) *surface force field* and (3) *surface adsorption*. Contributions of these effects on gas transport differ depending on the pore/channel size, gas pressure, gas–surface interactions and chemistry. While rarefaction effects can be estimated using kinetic theory (KT)-based procedures such as solution of the Boltzmann transport equation or direct simulation Monte Carlo, surface force field and adsorption effects require molecular-level resolution mostly accessible by molecular dynamics (MD).

Gas flows evolve through intermolecular collisions determined by the mean free path, which is an intrinsic length scale for momentum transport. Ratio of the mean free path to a characteristic length, such as the channel height, gives Knudsen number (*Kn*) that determines the degree of rarefaction, leading to continuum, slip, transition and free-molecular flow regimes (Karniadakis et al. 2005). MD simulations of gas flows require computational domains that are at least one mean free path long in the stream-wise and lateral directions in order not to suppress gas–gas collisions. This results in large simulation domains dominated by an excessive number of wall molecules, creating challenges for classical non-equilibrium MD. We addressed this problem by developing the smart wall molecular dynamics (SWMD) algorithm, which enabled MD simulations of nanoscale gas flows with 3D molecular surfaces for the first time in the literature (Barisik et al. 2010).

✉ Ali Beskok
abeskok@smu.edu

[1] Mechanical Engineering Department, Izmir Institute of Technology, 35430 Izmir, Turkey

[2] Mechanical Engineering Department, Southern Methodist University, Dallas, TX 75275-0337, USA

Using SWMD, we investigated shear- and force-driven nano-channel gas flows in the entire Knudsen regime (Barisik and Beskok 2010, 2011a, b, 2012, 2014, 2015). Simulation results have shown formation of a near-wall layer that is several molecular diameters thick. We identified this as the "wall force penetration length" (L_f), where the gas density and velocity distributions are under the effect of surface molecular forces. Transport beyond the near-wall region can be considered as the bulk flow region, which exhibits flow physics predictable by KT solutions for a prescribed tangential momentum accommodation coefficient (TMAC).

- In the near-wall region, there are significant variations in the gas density and velocity, while the shear and normal stresses are anisotropic (Barisik and Beskok 2011a). Ideal gas law is valid in the bulk region.
- Transport in the bulk and near-wall regions is determined by the gas–wall interaction parameter and the Knudsen number (Barisik and Beskok 2011b; 2012, 2014, 2015).
- TMAC values are determined by the gas–wall interaction parameter, and they are independent of the Knudsen number (Barisik and Beskok 2011b, 2012).
- Surface adsorption of gas molecules can be characterized as a function of the gas–wall interaction parameter (Barisik and Beskok 2012).
- Mean free path of gas molecules are unaffected from nano-confinements in agreement with KT regardless of the molecular surface forces and adsorption. Comparison of the velocity profiles obtained in MD with the linearized Boltzmann solutions at predicted *Kn* values shows good agreement in the bulk of the channels, while deviations in the near-wall region due to the influence of surface are observed (Barisik and Beskok 2015).

These results clearly show that depending on the characteristic dimensions of the confinement, surface van der Waals forces can dominate nano-channel flows. In order to identify the effects of the near-wall region, we introduced a new dimensionless parameter B as the ratio of the wall force penetration length to the channel height ($B = L_f/H$) and investigated nanoscale gas flows at various B values to explore similitude of nano-flows with rarefied gas flows. Results showed dynamic similarity between the two for $B \to 0$, where the near-wall region had very limited effect on the mass transport with the exception of determining the TMAC value, which is the boundary condition for KT solutions. For finite B values, the near-wall region covers larger portions of the flow domain exhibiting increased deviations from KT solutions and eventually resulting in cases where the bulk flow region completely disappears (Barisik and Beskok 2014).

Objectives of this paper are twofold. First, we present the universal behavior of gas velocity distribution in the near-wall region as functions of the Knudsen number and the gas–wall interaction parameter. Then, we outline a procedure that can be used to correct kinetic-theory-based gas mass flow rate predictions in the literature as a function of B parameter and MD data, enabling scale-based corrections for nano-channel gas flows.

2 Three-dimensional MD simulation details

Argon gas flow between two parallel surfaces was modeled using SWMD. The SWMD is an MD algorithm calculating evolution of molecules based on Newton's second law and intermolecular forces with a special subroutine for gas–surface interactions (Barisik et al. 2010). We simulated force-driven isothermal flows, which are hydrodynamically similar to pressure-driven gas flows at low Mach numbers (Ma). Computational domain was periodic in the stream-wise and lateral directions and extended one mean free path (λ_{Ar}) in these directions. Thermodynamic state of argon was fixed at 298 K and 113.4 kPa, which corresponds to a density of $\rho_{Ar} = 1.896$ kg/m^3 and $\lambda_{Ar} = 54$ nm. By keeping gas temperature at 298 K, pressure was varied to obtain different λ values. Mean molecular spacing for each case was checked, and the thermodynamic states were validated to be dilute gas, obeying the ideal gas law. A constant driving force (F_{drive}) was applied on each gas molecule in the stream-wise direction, while the magnitude of the force was controlled to maintain $Ma < 0.1$, so that gas flow is nearly incompressible.

Lennard–Jones (L–J) 6–12 potential was used to model van der Waals interactions between gas–gas and gas–wall molecules. The truncated 6–12 L–J potential is given as

$$V_{\text{truncated}}(r_{ij}) = 4\varepsilon\left(\left(\left(\frac{\sigma}{r_{ij}}\right)^{12} - \left(\frac{\sigma}{r_{ij}}\right)^{6}\right) - \left(\left(\frac{\sigma}{r_c}\right)^{12} - \left(\frac{\sigma}{r_c}\right)^{6}\right)\right), \quad (1)$$

where r_{ij} is the intermolecular distance, ε is the depth of the potential well, σ is the molecular diameter and r_c is the cut-off radius. In this study, we utilized $r_c = 1.08$ nm, which is approximately equal to 3.17σ for argon molecules. At this cutoff distance, the attractive part of the L–J potential was reduced to 0.00392ε. Our algorithm utilized the well-known link cell method to handle particle–particle interactions (Allen and Tildesley 1989). Mass for an argon molecule is $m_{Ar} = 6.63 \times 10^{-26}$ kg, its molecular diameter is $\sigma_{Ar} = 0.3405$ nm and the depth of the potential well for argon is $\varepsilon_{Ar} = 119.8 \times k_b$, where k_b is the Boltzmann constant (1.3806×10^{-23} J K^{-1}). Here, ε_{Ar} defines the gas–gas

interaction strength and is identified as ε_{ff}. During simulations, argon–wall interactions (ε_{wf}) use ε_{Ar}, $2\varepsilon_{Ar}$ and $3\varepsilon_{Ar}$ to investigate increasing wall attraction. We present our results as a function of the normalized interaction parameters, which result in $\varepsilon_{wf}/\varepsilon_{ff} = 1$, 2 and 3 for gas–wall interactions. Walls were modeled molecularly using face-centered cubic (FCC) structure with (1,0,0) plane facing the gas. For simplicity, walls molecules have mass and diameter equivalent to argon ($m_{wall} = m_{Ar}$, $\sigma_{wall} = \sigma_{Ar}$). Since wall molecules are fixed in the cold wall model, the wall's molecular mass has no effect in momentum exchange between the gas and wall molecules. In addition, the molecular diameter between different species does not vary drastically.

Simulations started from the Maxwell–Boltzmann velocity distribution for gas molecules at 298 K. Initial particle distribution was evolved 10^6 time steps (4 ns) to reach an isothermal steady state using 4 fs (~0.002τ) time steps, after which 8×10^6 time steps (32 ns) were performed for time averaging. Longer time averaging has also been performed to confirm convergence of density, stress and velocity profiles to steady state. In order to capture variations within the near-wall region accurately and using same resolution for each channel case, all simulation domains were divided into slab bins with constant height of 0.054 nm in the wall normal direction. Canonical ensemble (NVT, i.e., constant mole, N, volume, V and temperature, T) was performed by utilizing a thermostat. We employed the Nose–Hoover algorithm (Evans and Hoover 1986) as a global thermostat inside the local sub-domains to obtain isothermal conditions at 298 K with a relaxation time of ~0.2 ps. Sub-domains have 0.54 nm heights through the entire span, which is 10 times larger than the utilized bin size. Local gas temperature was also computed throughout the channels to ensure isothermal conditions were imposed by the thermostat.

The probable statistical effects of the number of simulated molecules are checked by measuring the molecular velocity distribution and the statistical fluctuations in the system. We compared the MD measured gas velocity distribution with theoretical Maxwell–Boltzmann prediction at the corresponding gas temperature. Regardless of the channel height, density, surface potential and flow conditions, MD gas velocity distribution is found identical to the kinetic theory description, which shows that local thermal equilibrium is maintained for these isothermal cases regardless of the nanoscale confinement effects induced by molecular surfaces. The 32 ns averaging performed is considered excessively long for a classical MD system. Very low fluctuations in the velocity and density profiles resulted in negligible standard deviations in the results.

3 Results and discussion

Force-driven rarefied gas flows between parallel plates separated by a distance H show Kn dependent variation in mass flow rate, which also exhibits the well-known Knudsen's minimum around $Kn = 1$ (Knudsen 1909). In order to associate our MD results with kinetic theory predictions, we need to define proper scales for normalization of the results. Mass flow rate for two-dimensional force-driven flows scale as $\ln(Kn)$ for $Kn \to \infty$, which is inappropriate to obtain relevant scales for normalization. On the other hand, three-dimensional rarefied gas flows in ducts and pipes give constant mass flow rate in the free-molecular limit that is scalable by

$$\dot{M}_{FM} = \frac{H^2}{\sqrt{2R_{Ar}T_{Ar}}}\rho_{Ar}\frac{F_{drive}}{m_{Ar}}, \tag{2}$$

where $\dot{M}_{FM}$ is the mass flow rate per unit width; ρ_{Ar}, R_{Ar} and T_{Ar} are the argon density, specific gas constant and temperature, respectively, and F_{drive} is the driving force on each molecule. Using Eq. (2), one can obtain channel-averaged free-molecular velocity as $\bar{u}_{FM} = \dot{M}_{FM}/H\rho_{Ar}$. Sharipov obtained linearized Boltzmann (LB) equation solutions between two parallel plates at various Knudsen numbers and TMAC values and reported mass flow rates normalized using Eq. (2). Table 1 presents kinetic theory predictions of normalized mass flow rate per unit channel width M_k^* for TMAC = 0.75 as a function of the modified Knudsen number $k = (\sqrt{\pi}/2)Kn$. For fixed density and channel height, M_k^* can also be interpreted as the ratio of the mean velocity at a given k value ($\bar{u}_k$) and $\bar{u}_{FM}$.

Although velocity profiles for TMAC = 1 flows at various Kn values exist in the literature, we could not find published velocity profiles for TMAC = 0.75 flows. Therefore, we had to resort to Beskok–Karniadakis model (BKM), which is a phenomenological model for pressure-driven pipe and rectangular duct flows (Beskok and Karniadakis 1999). BKM is valid for low Mach number compressible gas flows, where the flow is nearly isothermal, and it accurately describes the velocity profile, shear stress, pressure

Table 1 Linearized Boltzmann calculations of mass flow rate per unit channel width (M_k^*) for TMAC = 0.75 flows [data adopted from Sharipov (2001)]

	k = 0.236	k = 0.5	k = 1	k = 5	k = 10
M_k^*	2.383	2.203	2.150	2.429	2.655
$j_{L_f,k}^*$	1.173	1.173	1.180	1.222	1.277

Normalized average mass flux in the near-wall region $\left(j_{L_f,k}^*\right)$ for various k flows, predicted by MD simulations using $\varepsilon_{wf}/\varepsilon_{ff} = 1$

gradient and mass flow rate in the entire Knudsen regime (Beskok and Karniadakis 1999). Using only two fitting parameters, BKM captures Maxwell's first-order slip model in the slip flow regime and reaches free-molecular flow results for $Kn \to \infty$. An essential component of the model is approximation of the velocity profile using a parabola and a generalized slip model, which was verified using variable hard sphere model DSMC algorithm and LB results for TMAC = 1.0, as well as an asymptotic analysis of Burnett equations for pressure-driven channel flows (Beskok 1996; Beskok and Karniadakis 1994). Velocity distribution for pressure-driven isothermal gas flow between two parallel plates separated by a distance H is a function of the local pressure gradient, gas viscosity, k and TMAC values, and it varies both in the stream-wise direction (x) and across the channel (y). Effects of the stream-wise variations can be canceled if the velocity profile is normalized by the local mean velocity ($\bar{u}_k$), resulting in a model that accurately approximates the normalized velocity distribution as a function of k, y and TMAC as,

$$U^*(Y,k) \equiv \frac{u(x,y)}{\bar{u}_k} = \left[\frac{-Y^2 + Y + \left(\frac{2-\mathrm{TMAC}}{\mathrm{TMAC}}\right)\frac{2k}{\sqrt{\pi}+2k}}{\frac{1}{6} + \left(\frac{2-\mathrm{TMAC}}{\mathrm{TMAC}}\right)\frac{2k}{\sqrt{\pi}+2k}}\right], \tag{3}$$

where $Y = y/H$. This equation properly considers rarefaction effects and can be applicable for nanoscale flows with negligible surface force effects when $B \to 0$, which is the limit of dynamic similarity between rarefied and nanoscale flows, so that kinetic theory solutions are applicable. However, for B values different than zero, transport is affected by the surface force field, which should be considered using atomistic simulations.

In order to study gas flows in nano-confinements, we began investigations with $k = 1$ flows in the transition flow regime. Simulation snapshots provided in Fig. 1 show molecularly modeled gas and solid surfaces. A wide range of conduit sizes are investigated. We simulated 5.4, 8.64, 10.8, 16.4, 21.6, 27 and 54 nm height channels, while different $k = 1$ flows were established by varying the gas pressure. For example, in a 54-nm channel, argon gas at standard conditions resulted in $k = 1$. Gas pressure was increased ten times to reach $k = 1$ flow in 5.4 nm channel. Driving force on each molecule (F_{drive}) was determined using integral momentum equation applied to different sized control volumes to keep maximum channel velocity approximately a constant, which required variations as a function of the cross-sectional area. For example, $F_{\mathrm{drive}} = 4.037 \times 10^{-14}$ N/atom was used for the 5.4 nm height channel (5.4 nm × 54 nm flow area), while

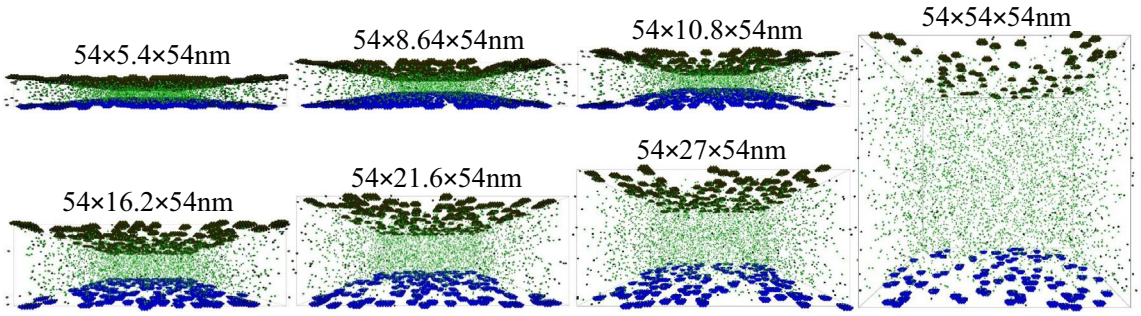

Fig. 1 Simulation snapshots of 5.4, 8.64, 10.8, 16.2, 21.6, 27 and 54 nm height channels

Table 2 Simulation parameters for each channel height for $k = 1$ flows

Height (nm)	B (L_f/H)	Density (kg/m^3)	k	F_{drive} (N/Atom)	Molecular dynamics		
					τ_{wall} (kPa)	M_{MD} (kg/sm)	$j^*_{L_f,k=1}$
5.4	0.2	18.252	1.0	4.037E−14	29.107	14.45×10^{-7}	1.19
8.64	0.125	11.559	1.0	2.523E−14	19.057	17.88×10^{-7}	1.18
10.8	0.1	9.291	1.0	2.019E−14	15.235	18.57×10^{-7}	1.21
16.2	0.066	6.235	1.0	1.346E−14	10.254	19.32×10^{-7}	1.19
21.6	0.05	4.691	1.0	1.009E−14	7.783	19.64×10^{-7}	1.17
27	0.04	3.761	1.0	8.075E−15	6.225	19.82×10^{-7}	1.15
54	0.02	1.887	1.0	4.037E−15	3.116	20.20×10^{-7}	1.20

MD measurements of wall shear stress, mass flow rate per unit depth and free-molecular normalization of the average mass flux $\left(j^*_{L_f,k=1}\right)$ inside the wall force penetration depth (~3σ) are given for each case

$F_{\text{drive}} = 4.037 \times 10^{-15}$ N/atom was used for the 54 nm channel case (54 nm × 54 nm flow area), as given in Table 2.

Non-dimensional gas velocity profiles (u^*) for $k = 1$ flows in different height channels are shown in Fig. 2 as a function of the normalized channel height $Y = y/H$. Channel center is at $Y = 0.5$, while the centers of wall molecules on the bottom wall are lined at $Y = 0.0$. MD-based velocity profiles were normalized using $\bar{u}_{\text{FM}}$, while BKM predictions from Eq. (3) with TMAC = 0.75 were multiplied with $M^*_{k=1} = 2.15$ for consistent normalization. Results in Fig. 2 show good agreement between the MD data and the BKM predictions *sufficiently away from the walls* for channel heights greater than 5 nm. The 8.64 nm height case given in Fig. 2a is found as the dimensional limit of this agreement between the nanoscale gas flow bulk velocity and KT predictions. Kinetic-theory-based solutions cannot explain bulk velocity of nano-channels smaller than 8.64 nm for the current MD system (Barisik and Beskok 2014). Different than the BKM, MD further calculates surface force and surface adsorption in addition to gas rarefaction. Hence, MD results deviate from KT solution near the surfaces. These deviations are mostly confined inside the wall force penetration regions (L_f). Nearly parabolic velocity profiles are observed in the bulk flow region with significant variations within the L_f. Since the dimension of the near-wall region remains constant ($L_f = 3\sigma \approx 1$ nm in this study due to the utilized van der Waals surface forces), its influence on transport becomes increasingly significant with decreased channel heights, which correspond to increased B values.

Results in Fig. 2 show presence of an outer scaling in the velocity profiles where MD results match BKM model approximately $2B$ distance away from the surfaces. However, there are significant differences between MD results and BKM in the near-wall region. Figure 3a, b shows variations of normalized gas density and velocity as a function of the inner-scaling based on molecular diameter, σ. We call this wall units $y^* = y/\sigma$; therefore, $y^* = (H/\sigma)Y$. In the figure,

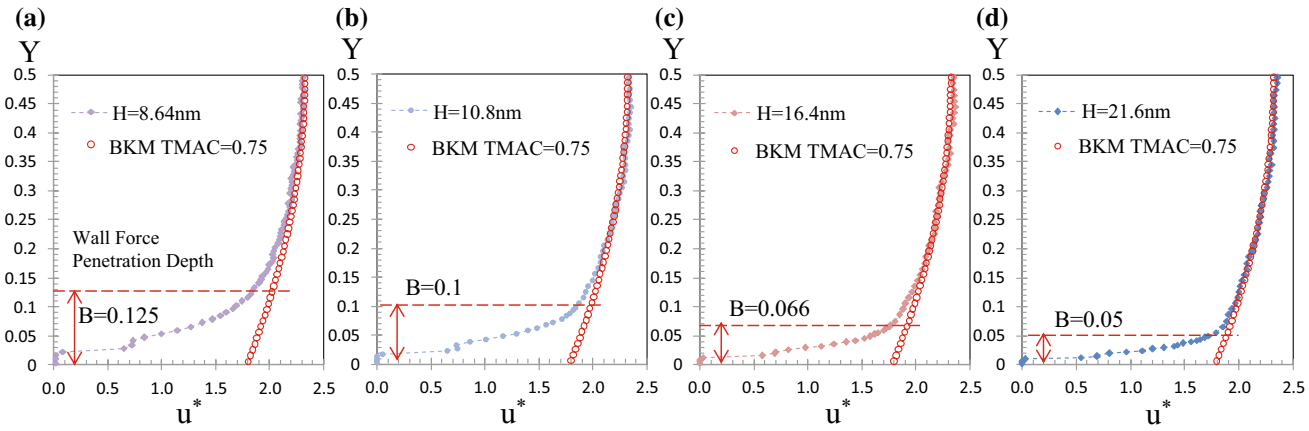

Fig. 2 Dimensionless velocity profiles for $k = 1$ flows as a function of normalized channel height Y, corresponding to different B values

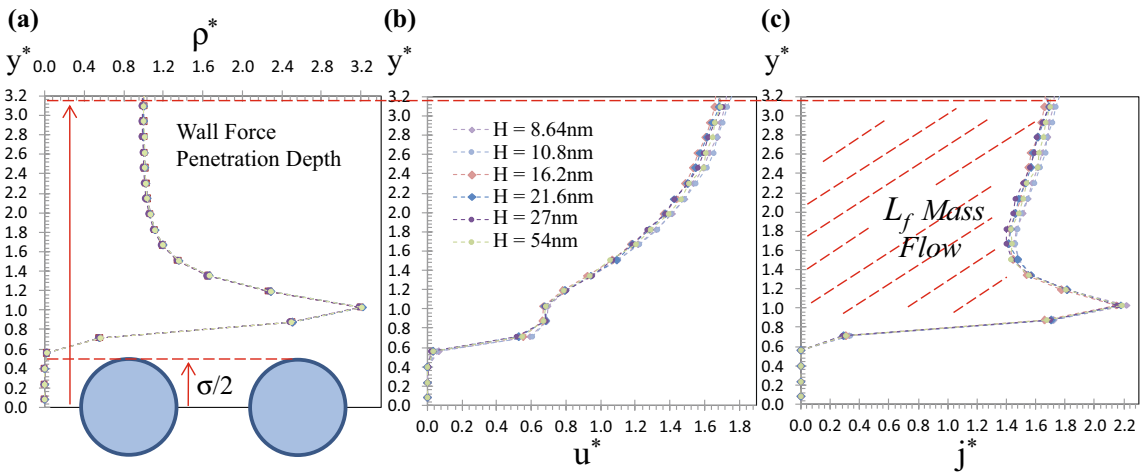

Fig. 3 Normalized density (**a**), velocity (**b**) and mass flux (**c**) distributions within the wall force penetration region for $k = 1$ flows in different height channels. **a** Illustration of surface molecules to demonstrate wall penetration into the flow domain

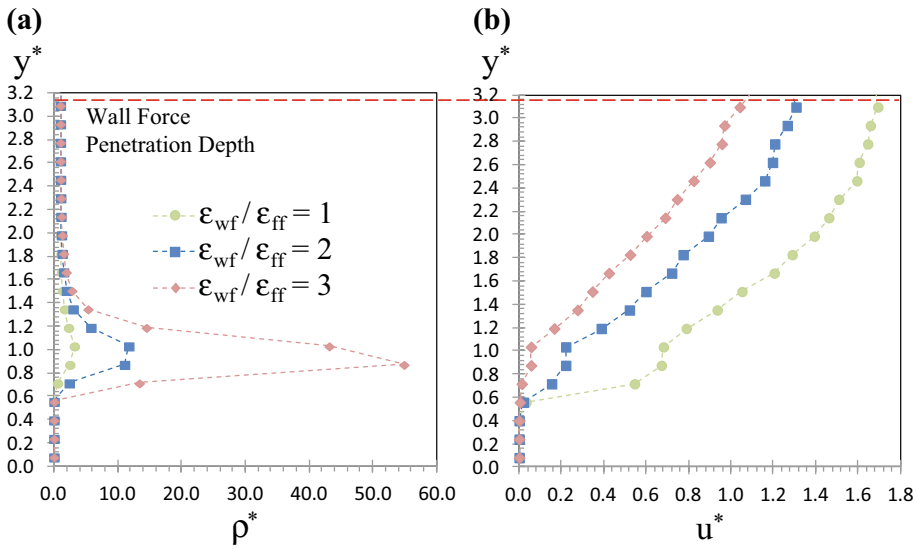

Fig. 4 Normalized density (**a**) and velocity profiles (**b**) in the near-wall region obtained at various gas–wall interaction strengths for $k = 1$ flows

density is normalized by the channel bulk value, while MD-based velocity profiles are normalized by $\bar{u}_{\mathrm{FM}}$. Results from six different channel height cases are presented. Regardless of the channel dimensions, normalized density and velocity profiles show *universality* for $y^* \leq 3$ for $k = 1$ flows. Near-wall normalized density, velocity and mass flux distributions are independent of the local thermodynamic state, channel dimensions and the applied force. This universal behavior can be identified as "the law of the nano-wall." For $3 \leq y^* \leq 6$, the inner-layer velocity distribution transitions to match the outer layer velocity scaling, while reasonable match between the BKM and MD results is obtained $Y = 2B$ distance from the wall, which corresponds to $y^* = 6$ in wall units.

Figure 4 shows normalized density and velocity profiles in the near-wall region for different gas–wall interaction strengths ($\varepsilon_{\mathrm{wf}}/\varepsilon_{\mathrm{ff}}$), resulting in TMAC = 0.75, 0.9 and 0.94 for $\varepsilon_{\mathrm{wf}}/\varepsilon_{\mathrm{ff}} = 1$, 2 and 3, respectively (Barisik and Beskok 2012). Near-wall density profiles peak around $y^* = 1$ and then reach bulk flow value around $y^* = 2$. The peak density increases with $\varepsilon_{\mathrm{wf}}/\varepsilon_{\mathrm{ff}}$ due to strong wall attraction and eventually leads to monolayer adsorption on the surface. Gas velocity around $y^* = 1$ is nearly zero for the $\varepsilon_{\mathrm{wf}}/\varepsilon_{\mathrm{ff}} = 3$ case, showing onset of gas adsorption. It is important to indicate that $\varepsilon_{\mathrm{wf}}/\varepsilon_{\mathrm{ff}} = 1$ and 2 cases allow gas slip on atomistically smooth surface. Although the near-wall density profile is independent of the Knudsen number, velocity distribution shows dependence on both $\varepsilon_{\mathrm{wf}}/\varepsilon_{\mathrm{ff}}$ and local k; it is not scalable with the TMAC values.

Mass flow rate Predictions Presence of *universal near-wall* density and velocity distributions enables corrections of KT-based mass flow rate results for finite B values. Mass flow rate in a nano-channel for certain k flow $\left(M^*_{\mathrm{Nano},k}\right)$ can be calculated as follows

$$M^*_{\mathrm{Nano},k} = M^*_k - 2M^*_{L_{\mathrm{f}},k} + 2M^*_{L_{\mathrm{f}},\mathrm{Nano}} \tag{4}$$

where M^*_k is the mass flow rate form KT at a given k value (Table 1), and $M^*_{L_{\mathrm{f}},k}$ is the mass flow rate within the force penetration region (L_{f}) calculated from KT, while $M^*_{L_{\mathrm{f}},\mathrm{Nano}}$ is the mass flow rate within L_{f} calculated by SWMD. Factor of 2 is required to consider top and bottom surfaces of the channel. Equation (4) is a hybrid mass flow rate model correcting KT calculations by considering nanoscale surface effects using MD data from the near-wall region. This correction is only possible by properly characterizing the velocity and density profiles from KT and MD and then by integrating them within their respective domains. First, we evaluate the KT mass flow rate within the force field penetration depth ($L_{\mathrm{f}} \approx 3\sigma$) as,

$$M^*_{L_{\mathrm{f}},k} = \left(\int_0^B U^*(Y,k)_{\mathrm{BKM}} \mathrm{d}Y \right) \times M^*_k, \tag{5}$$

where U^* is the BKM velocity profile from Eq. (3), and M^*_k is required to properly scale BKM as described earlier. Mass flow rate within the near-wall region is obtained by numerical integration (trapezoidal rule) of MD simulation data using

$$M^*_{L_{\mathrm{f}},\mathrm{Nano}} = \left(\frac{\sigma}{H} \int_0^{L_{\mathrm{f}}/\sigma} \rho^* u^* \mathrm{d}y^* \right), \tag{6}$$

where $\rho^* = \rho/\rho_o$. Upper limit of the integral uses L_{f}/σ, which is $y^* = 3$ in this study. Although $M^*_{L_{\mathrm{f}},\mathrm{Nano}}$ changes with the channel size, value of the integral in Eq. (6) is constant in the wall coordinates for a given k and gas–wall interaction strength. It is possible to define an averaged mass flux $j^*_{L_{\mathrm{f}},k}$ in the near-wall region, which simplifies Eq. (6) as

$$M^*_{L_{\mathrm{f}},\mathrm{Nano}} = B \times j^*_{L_{\mathrm{f}},k}. \tag{7}$$

Values of $j^*_{L_{\mathrm{f}},k}$ for $k = 1$ flow are given in Table 2 for various channels. As expected, the average near-wall mass flux

is constant regardless of the channel dimensions. Figure 3c shows normalized mass flux distribution in the near-wall region for six different height channels, verifying this universal distribution. Equations (4–7) constitute Beskok–Barisik correction for nanoscale mass flow rate, which can be incorporated to any kinetic-theory-based mass flow rate database, as shown here.

We applied Beskok–Barisik correction (BBC) on the listed $k = 1$ flow cases with channel heights varying between 5.4 and 54 nm. MD measured mass flow rate, KT prediction and BBC for each case are given in Fig. 5 as a function of parameter B. MD measured mass flow rate in 54 nm channel ($B = 0.02$) agrees well with KT prediction. Similar to earlier discussions, KT solutions do not require any correction when B is negligibly small. As B increases, percentage of L_f region compared to flow domain increases making nanoscale surface effects dominant. Percentile differences for each channel case are listed in Table 3 where KT overestimates the mass flow rate 37 and 12 % in 5.4 and 8.64 nm channels, respectively. Alternatively, when we use BBC to correct KT results, we can successfully calculate nano-channel mass flow rates in channels as small as 8.64 nm with 2.5 % error. Details of BBC calculation, percentile contributions of each term and the differences between MD measurements and the result of BCC are given in Table 3. On a side note, 5.4-nm-channel flow rate cannot be predicted by BBM since the bulk velocity does not match with KT solutions anymore due to large surface force field effects. In an earlier study, this behavior was investigated and the dominance of surface effects over rarefaction was presented in the entire Knudsen regime (Barisik and Beskok 2014).

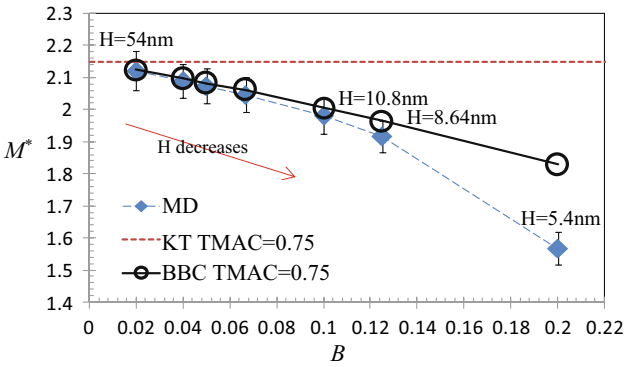

Fig. 5 Normalized MD mass flow rates for $k = 1$ flows as a function of B parameter at various channel heights compared with KT predictions and KT with BBC using Eqs. (4–7)

In order to investigate the velocity distribution in the near-wall region at different Knudsen values, we simulated $k = 0.286$, 0.5, 1, 5 and 10 flows inside a 10.8-nm height channel and computed mass flux inside the L_f region using Eq. (6). Figure 6a shows normalized velocity distribution in the near-wall region for various k values spanning from late slip to free-molecular flow regimes. This inner velocity scaling is a function of k for $\varepsilon_{wf}/\varepsilon_{ff} = 1$. Density distributions in nano-channels at different k flows are identical with data shown in Fig. 3a, since the near-wall density variation is affected only by the gas–wall interaction parameter ($\varepsilon_{wf}/\varepsilon_{ff}$). Combining the local density and velocity profiles, we obtained average mass flux in the near-wall region $\left(j^*_{L_f,MD}\right)$, whose variation is shown in Fig. 6b for different k flows and its numerical values are presented in Table 1.

Using Sharipov's mass flow rate data obtained for TMAC = 0.75 flows (Sharipov 2001), and the near-wall average mass flux presented in Table 1, we imposed Beskok–Barisik correction to the KT data for 10.8 nm height channels, where $B = 0.1$. Figure 7 shows normalized mass flow rate obtained using MD, KT and BBC. Proposed model shows reasonable agreements with MD data, enabling size-dependent corrections to mass flow rate predicted by kinetic

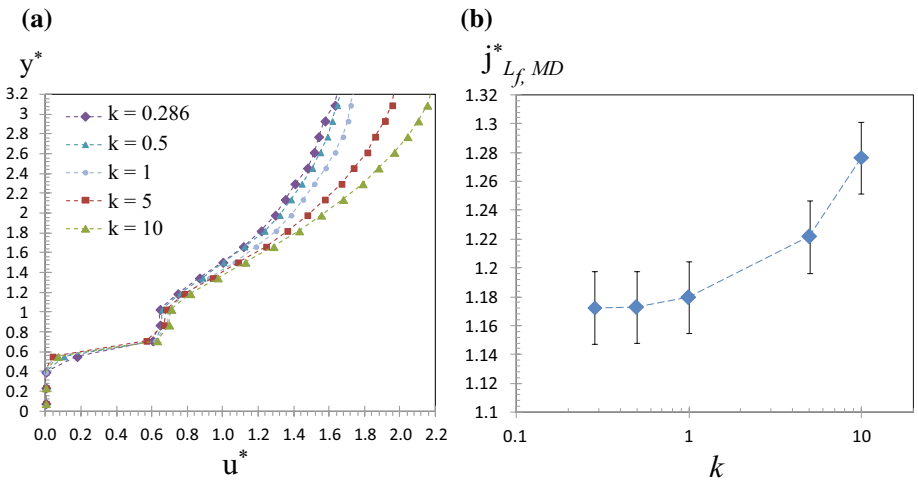

Fig. 6 Normalized velocity distribution (**a**) and average mass flux within the wall force penetration region (**b**) for various Knudsen flows

Table 3 Calculation of nanoscale gas mass flow rate using Eqs. (4–7) in various height nano-channels for $k = 1$ flow

Height (nm)	B (L_f/H)	$\frac{M_{KT}-M_{MD}}{M_{MD}}$ %	$M^*_{L_f,k}/M^*_k$ %	$M^*_{L_f,Nano}/M^*_k$ %	$\frac{M_{Nano}-M_{MD}}{M_{MD}}$ %
5.4	0.2	−37.00	18.44	10.98	−16.55
8.64	0.125	−12.17	11.16	6.86	−2.52
10.8	0.1	−8.53	8.82	5.49	−1.29
16.2	0.066	−5.01	5.71	3.66	−0.70
21.6	0.05	−3.64	4.3	2.74	−0.41
27	0.04	−2.89	3.42	2.2	−0.36
54	0.02	−1.34	1.69	1.1	−0.13

Third column shows error in KT results, while the last column shows error in BBC. The fourth and fifth columns are percentile contributions from Eqs. (5) and (7), respectively

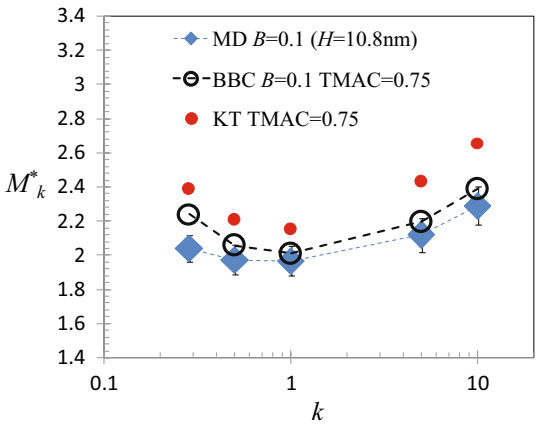

Fig. 7 Free-molecular scaling of MD measured mass flow rates inside 10.8 nm height channel compared with predictions of KT and KT with BBC (Eqs. 4–7) as a function of k

theory calculations for a wide range of Knudsen numbers. Differences between the MD and BBC are primarily induced by the fact that inner-layer scaling of the velocity profiles transitions to bulk flow approximately $2B$ distance away from the surfaces (Fig. 2). However, BBC uses the near-wall mass flux, which is universal only in the wall force penetration region. This creates a small error in the BBC. In addition, BKM approximates the KT-based velocity profiles as parabolic (Eq. 3), which has some error for $k \approx 1$ [see Figures 4.19 and 4.20 in Karniadakis et al. (2005)].

4 Conclusions

SWMD results obtained for force-driven gas flows in a wide range of Knudsen values show near-wall and bulk flow regions. While the density and velocity distributions in the near-wall region are determined by the gas–wall interaction parameter, velocity distribution also depends on the local Knudsen number. Near-wall normalized density, velocity and mass flux distributions are independent of the local thermodynamic state, channel dimensions and the applied force. This universal behavior can be identified as "the law of the nano-wall." For $B \leq 0.125$, one could identify a bulk flow region that matches kinetic-theory-based solutions. Considering that the near-wall region exists on both surfaces of the channel, near-wall effects are present in 25 % of the domain for $B = 0.125$. For smaller channels, the bulk flow region does not follow kinetic theory solutions.

We outlined a procedure that can be used to correct kinetic-theory-based mass flow rate predictions in the literature for nanoscale effects as a function of the B parameter. The method uses dimensionless velocity profiles from Beskok–Karniadakis model (Beskok and Karniadakis 1999) to subtract the non-dimensional near-wall mass flux from KT solutions and corrects it using that predicted by SWMD. This correction, valid for $B \leq 0.125$, results in accurate mass flow rate predictions for nano-channels. Overall, the proposed methodology can be adopted to correct kinetic-theory-based flow rate data for nanotubes and channels, which can have profound impacts in predicting gas transport in nano-channels, tubes and nano-porous media.

Acknowledgments Murat Barisik would like to thank H2020 Marie Skłodowska-Curie action CO-FUNDED Brain Circulation Scheme for support under the Grant Number TÜBİTAK 115C026. Ali Beskok would like to thank American Chemical Society (ACS) for support under the Grant Number 54562-ND9.

References

Allen MP, Tildesley DJ (1989) Computer simulation of liquids. Oxford University Press, New York

Barisik M, Beskok A (2010) MD simulations of nano-scale gas flows: a case study of couette flow at $Kn = 10$. In: Proceedings of the 27th symposium on rarefied gas dynamics Pacific Grove, California, July 10–15

Barisik M, Beskok A (2011a) Equilibrium molecular dynamics studies on nanoscale-confined fluids. Microfluid Nanofluidics 11(3):269–282. doi:10.1007/s10404-011-0794-5

Barisik M, Beskok A (2011b) Molecular dynamics simulations of shear driven gas flows in nano-channels. Microfluid Nanofluidics 11(5):611–622. doi:10.1007/s10404-011-0827-0

Barisik M, Beskok A (2012) Surface–gas interaction effects on nanoscale gas flows. Microfluid Nanofluidics 13(5):789–798. doi:10.1007/s10404-012-1000-0

Barisik M, Beskok A (2014) Scale effects in gas nano flows. Phys Fluids Phys Fluids 26:052003. doi:10.1063/1.4874678

Barisik M, Beskok A (2015) Molecular free paths in nano-scale gas flows. Microfluid Nanofluidics 18(5–6):1365–1371. doi:10.1007/s10404-014-1535-3

Barisik M, Kim B, Beskok A (2010) Smart wall model for molecular dynamics simulations of nanoscale gas flows. Commun Comput Phys 7:977–993

Beskok A (1996) Simulations and models for gas flows in microgeometries. Ph.D. Thesis, Princeton University, Princeton, New Jersey

Beskok A, Karniadakis GE (1994) Simulation of heat and momentum transfer in complex micro-geometries. J Thermophys Heat Transf 8(4):647–655

Beskok A, Karniadakis GE (1999) A model for flows in channels, pipes and ducts at micro and nano scales. Microscale Thermophys Eng 3(1):43–77

Chalk SG, Miller JF (2006) Key challenges and recent progress in batteries, fuel cells, and hydrogen storage for clean energy systems. J Power Sour 159:73–80

Cho JH, Yang SJ, Lee K, Park CR (2011) Si-doping effect on the enhanced hydrogen storage of single walled carbon nanotubes and graphene. Int J Hydrogen Energy 36:12286–12295

Chong KK, Grieser W, Passman A, Tamayo H, Modeland N, Burke B (2010) A Completions guide book to shale-play development: a review of successful approaches toward shale-play stimulation in the last two decades. In: Canadian unconventional resources and international petroleum conference. doi:10.2118/133874-MS

Evans DJ, Hoover WG (1986) Flows far from equilibrium via molecular-dynamics. Annu Rev Fluid Mech 18:243–264

Furukawa H, Yaghi OM (2009) Storage of hydrogen, methane, and carbon dioxide in highly porous covalent organic frameworks for clean energy applications. J Am Chem Soc 131(25):8875–8883

Juang JY, Bogy DB, Bhatia CS (2007) Design and dynamics of flying height control slider with piezoelectric nanoactuator in hard disk drives. ASME J Tribol 129(1):161–170

Karniadakis GE, Beskok A, Aluru N (2005) Micro flows and nano flows: fundamentals and simulation. Springer, New York

Knudsen M (1909) Die Gesetze der Molekularstromung und der innern Reibungsstromung der Gase durch Rohren. Ann Phys 28:75–130

Li B, Jiang B, Fauth DJ, Gray ML, Pennline HW, Richards GA (2011) Innovative nano-layered solid sorbents for CO_2 capture. Chem Commun 47(6):1719–1721

Loucks RG, Reed RM, Ruppel SC, Jarvie DM (2009) Morphology, genesis, and distribution of nanometer-scale pores in siliceous mudstones of the Mississippian Barnett Shale. J Sediment Res 79(12):848–861

Michel G, Sigal R, Civan F, Devegowda D (2011) Parametric investigation of shale gas production considering nano-scale pore size distribution, formation factor, and non-Darcy flow mechanisms. In: SPE annual technical conference and exhibition

Sharipov F (2001) Application of the Cercignani–Lampis scattering kernel to channel gas flows. In: AIP conference proceedings (vol 585, p 347)

Tagawa N, Yoshioka N, Mori A (2007) Effects of ultra-thin liquid lubricant films on contact slider dynamics in hard-disk drives. Tribol Int 40:770–779

Venna SR, Carreon MA (2009) Highly permeable zeolite imidazolate framework-8 membranes for CO_2/CH_4 separation. J Am Chem Soc 132(1):76–78

Yave W, Car A, Wind J, Peinemann KV (2010) Nanometric thin film membranes manufactured on square meter scale: ultra-thin films for CO_2 capture. Nanotechnology 21(39):395301